Terrestrial temperature, sea levels and ice area links with solar activity and solar orbital motion

Valentina V. Zharkova[1,2] **and Irina Vasilieva**[2,3]

1 - Department of MPEE, Faculty of Engineering and Environment, University of Northumbria, Newcastle upon Tyne, NE1 8ST, UK
Email: valentina.zharkova@northumbria.ac.uk; valja46@gmail.com
2 - ZVS Research Enterprise Ltd., London, EC1V 2NX, UK
3 - Department of Solar Physics, Main Astronomical Observatory, Kyiv, Ukraine

Abstract

This paper explores the links between terrestrial temperature, sea levels and ice areas in both hemispheres with solar activity indices expressed through averaged sunspot numbers together with the summary curve of eigen vectors of the solar background magnetic field (SBMF) and with changes of Sun-Earth distances caused by solar inertial motion resulting from the gravitation of large planets in the solar system. Using the wavelet analysis of the GLB and HadCRUTS datasets two periods: 21.4 and 36 years in GLB, set and the period of about 19.6 years in the HadCRUTS are discovered. The 21.4 year period is associated with variations in solar activity defined by the summary curve of the largest eigen vectors of the SBMF. A dominant 21.4-year period is also reported in the variations of the sea level, which is linked with the period of 21.4 years detected in the GLB temperature and the summary curve of the SBMF variations. The wavelet analysis of ice and snow areas shows that in the Southern hemisphere it does not show any links to solar activity periods while in the Northern hemisphere the ice area reveals a period of 10.7 years equal to a usual solar acitviity cycle. The TSI in March-August of every year is found to grow with every year following closely the temperature curve, because the Sun moves closer to the Earth orbit owing to gravitation of large planets. (solar inertial motion, SIM). While the variations of solar radiation during a whole year have more steady distribution without a sharp TSI increase during the last two centuries. The additional TSI contribution caused by SIM is likely to secure the additional energy input and exchange between the ocean and atmosphere.

1. Introduction

The global temperature was shown to rise, in general, from 1850 and at an unprecedented pace after 1970s [1, 2, 3]. A few main external forcing are used in the Coupled Model Inter-comparison Project (CMIP) models: solar, volcanic and longer term linear trend (to represent the anthropogenic CO2). The abrupt hike in the terrestrial temperature, coincided with the unusual climate patterns observed globally (Monsoon) [4] as well as regionally (Indian Summer Monsoon (ISM): [4, 5, 6]. ENSO: [7, 8], North Atlantic Oscillation (NAO) [9]. There is also substantial evidence that physical conditions are also changing in the ocean [10, 11] and in the terrestrial atmosphere [12, 13].

According to [14] a substantial growth of ice in Antarctica occurred in 1550-1860 being likely represented by two waves. This increase of the ice in Antarctica was co-temporal with the little ice age which occurred in many parts of the Earth that confirms either the volcanic or solar . nature of the little ice age [14].

Prediction of the effects of ice area variations on the changes of the sea level are done by many authors based on a wide range of approaches and methods ([see, for example, [15, 16] and references therein). Although none of these prediction could not correctly reflect the precise interaction of the ocean and atmosphere, possibly, because the variations of ice areas are not related directly to the ocean models [17].

The estimations of the current loss of mass for the shores of Amudsen (ices of Pine-Island, Twaits, Smith, Pope and Kohler glacier vary from 1.4 to 2.9 cm per century [18, 19, 20]. The glacier Pine Island, which is the most variable one could lead to the increase of the sea level by 3.5-10 mm during the next 20 years [21, 22, 23].

The sea level increase owing to melting ice and snow occurring on the Earth, melting ice of Arctics and Antarctica and because of the thermal expansion of the water during its warming in the summer [24]. In this sense, the increase of the sea level is a direct consequence of the temperature increase [25, 26]. In particular, Rahmsfortr (2007) [25] developed a semi-empirical approximation for a connection of the temperature and sea level variations in the 20th century that was later explored in a number of papers [27, 28, 29, 30].

Naturally, there is a spatial variability of tropical Pacific Sea Surface Temperature (SST) leading to different forms of ENSO, especially, Central Pacific (CP) ENSO, which is the most important one. It is mainly dominated by the variability of SST around CP region [31]. For CP ENSO, atmospheric forcing plays the dominant role and it has an extratropical connection [32] over the periods a few century in the past [33].

The Sun is the primary source of the energy for the climate of the Earth and other planets. Although, any warming due to increased solar activity in 11-year cycles is not considered to be uniform [34], either within the at-

mosphere or at the ocean surface. However, the patterns and amplitudes of the derived responses in temperature and ocean levels, are still the subject of some uncertainty. A large response was found in the Pacific in boreal winter: a positive anomaly in the Bay of Alaska [35], and also a reduction in a sea levels near the date line at around 20–40 N latitudes with a positive anomaly south of the equator, which was interpreted as a strengthening of the SE trade winds crossing the equator, driving increased ocean upwelling and cooler equatorial temperatures [36].

Explosive volcanos are another form of natural contribution that have an enormous impact on the climate of the Earth, which involves the troposphere as well as the stratosphere [37]. The role of explosive volcanos shows a noticeable influence on the modelled ENSO [38]. It was also suggested that explosive volcanos during El Niño phase contribute to its duration, whereas the same during La Niña shortens the period counteracting to its duration.

For example, during the intervening period of 1976–1998, two major volcanos erupted during 1982 and 1991 that coincidentally matched active years of stronger solar cycles. That period also captured two full solar cycles, (numbers 21 and 22) starting from one solar minimum (1976) and ending with another minimum (1996). A study suggested separating the period of those two decades gives better insight on understanding some climate features [9] that is consistent with analysis of the sea surface temperatures (SSTs) which shows a strong La Nina (Cold Event, CE)-like signal when the Sun is more active. However, another SST analysis [39] shows a slightly warmer band of water across the tropical Pacific associated with peaks in a decadal signal (DSO) identified as in phase with solar activity. Thus, there is no clear picture of the SST response at solar maximum.

The paper by [34] pointed out that the timing is crucial to producing apparent discrepancies between different analyses of solar activity effects and how it may be used to test mechanisms proposed to explain solar-climate links, in the context of ENSO variability. They identify solar cycle signals in 155 years of global sea level pressure (SLP) and sea surface temperature (SST) data using a multiple linear regression approach.

Although, solar activity was shown to be described not only by averaged sunspot numbers but also by eigen vectors of the solar background magnetic field (SBMF) derived with the principle component analysis (PCA) from the synoptic magnetic maps captured by the full-disk magnetograph of the Wilcox Solar Observatory, US [40]. The modulus of the summary curve of the two principal components of SBMF fits rather closely the averaged sunspot numbers currently used as the solar activity index [40, 41, 42, 43].

However, the advantage of the new proxy of solar activity, the summary curve of two PCs, is provided by the fact that it not only provides the amplitudes and shapes of solar activity cycles but also captures the leading magnetic polarities in these cycles. Furthermore, by adding the other eigen vectors of SBMF linked to quadruple and sextuple magnetic field components, besides the two PCs associated with magnetic dipoles, it can replicate closer not only the sunspot index [43] but also the soft X-ray flux index associated with solar flares [42].

The solar activity was shown to be defined by the solar dynamo action in the two layers of the solar interior producing two magnetic waves having close but not equal periods of about 11 years. The interference of these two

magnetic waves leads to a grand period of about 350-400 years for their amplitude oscillations when the normal magnetic wave (and cycle) amplitudes approach grand solar minima (GSM) caused by the wave's beating effect [40]. Such grand periods coincide with the well-known GSMs such as the Maunder minimum (MM), Wolf's, Oort's and other grand minima [44]. In fact, similar to the previous GSM, the Maunder Minimum, in 2020 the Sun was shown to enter the period of a modern GSM lasting until 2053 [40, 45].

During the most recent GSM, MM, there was a reduction for solar radiation by about 3 W/m^2 [46] and the terrestrial temperature dropped by about 1C [47], which, in turn, was proxied by the absence of sunspots and active regions on the solar surface during the MM [44]. Although, the terrestrial temperature was found increasing since the Maunder minimum by 0.5C per century [48, 1], which was first assigned to the increase of solar activity producing a modern warming period [49]. However, from cycle 21 the solar activity systematically decreased which coincided with a decrease of the solar background magnetic field in the approach of the GSM [41, 40]. And indeed, from cycle 21 the solar activity systematically decreased that coincided with a decrease of the solar background magnetic field in the approach to the grand solar minimum (GSM) [40, 42].

On the other hand, in the past few hundred years the Sun has been shown to provide some additional radiation to the Earth by moving closer towards the Earth's orbit because of the solar inertial motion (SIM) caused by the gravitation of the large planets [50, 51, 52, 53]. These periodic variations of the Sun-Earth distance, and the solar irradiance, occur every 2100-2200 years, called Hallstatt's cycles, which were independently derived from the isotope abundances in the terrestrial biomass [54, 55]. In the current Hallstatt's millennial cycle, the Sun-Earth distances are decreasing from the MM until 2600 that leads to the increase of solar irradiance deposited to the atmosphere of the Earth (and other planets) [51, 53].

This SIM effect is shown to contribute to the terrestrial atmosphere heating [51, 53], in addition to any heating caused by the greenhouse gasses considered in the terrestrial models. However, the most notable effect of SBMF in the next few decades will come from a reduction of solar activity, or from the modern grand solar minimum (GSM), which started in 2020 and will last until 2053 [40, 45].

The studies by different authors (see, for example, [56, 47, 57] and references therein) addressed the role of natural factors (the sun and volcano) comparing to that from CO2 led linear anthropogenic contributions. [57] identifies that dominance of Central Pacific (CP) ENSO and associated water vapour feedback during that period play an important role that confirms the suggestions by Salby (2012) [56]. The possible mechanism could be initiated via a preferential alignment of NAO phase, generated by explosive volcanos. Recently, [58] have shown that the causal relationship between an increase of the terrestrial temperature and a growth of the CO2 abundances clearly indicates that the CO2 presence must be a consequence of the terrestrial temperature growth and not vice versa as assumed by the modern temperature models [3]. This leaves the question still open what are the major causes of the observed temperature variations on the Earth.

The aim of the current study is an attempt to establish possible links between the terrestrial temperature, sea level and ice area coverage with the

solar activity, solar eigen vectors derived from the SBMF and the positions of the Sun in the planetary orbit following its inertial motion imposed by large planets of the solar system.

2. Observations

2.1. The datasets of terrestrial temperatures

There are numerous datasets of the terrestrial temperatures of different duration and quality of measurements.For the current study we consider reliable series of terrestrial temperature measurements, which satisfy the following conditions:

- should have a stable temperature scale;

- should have a global coverage of the terrestrial regions and this coverage should not be affected by the local phenomena, like North Atlantic Oscillation (NAO), or El Nino/La NIna events in the Pacific ocean area.

The temperature series reasonably complying with these conditions are the following. The first set is developed by the British Meteorological Center in Hadley and the department of Climate Research of the East Anglia University [$https://www.metoffice.gov.uk/hadobs/hadcrut5/$, accessed on 12/06/2023. This series starts from 1850 and named as HadCRUT5 for the future reference. The second set is the series of the surface temperature (GISSTEMP) produced by the NASA Goddard Institute of Space Science (GISS) $https://data.giss.nasa.gov/gistemp/tabledata_v4/GLB.Ts+dSST.txt$ accessed 12/06/2023 [59]. This set starts from 1880 and we will name it as GLB hereafter.

It can be seen that the two datasets are rather close besides in the interval of 1880-1910 when the GLB set has systematically higher magnitudes. The difference between these two series seems to be not so large as shown in Fig. 1, although it leads to some noticeable discrepancies revealed during the analysis of the periodic part of the series discussed below. In order to exclude the effects of limited lengths of the series, let us restrict ourselves by the interval of 1880-2022 covering the both temperature series.

2.2. Comparison of the sea levels and temperature variations

The series of temporal variations of the global mean sea level (GMSL) during 1880-2014 was obtained from the Centre for Protection of the Environment of the USA and SCIRO (Centre for Scientific and Industrial Research Organisation) ($http://www.cmar.csiro.au/sealevel/sl_data_cmar.html$. accessed on 29/07/2023. The detailed description the data is presented by [60].

The GLB temperature variations are shown in Fig. 2 (top plot) with the measured variations shown by the black line and thee averaged variations expressed by the 4th order polynomial by the red line. The sea level variations are shown in Fig. 2 (middle plot) with real measurements shown by the black line and the averaged ones by the 4th order polynomial shown by the red line. In Fig. 2 (bottom plot) the de-trended sea level variations, calculated by subtracting from the real data defined by the black curve, the
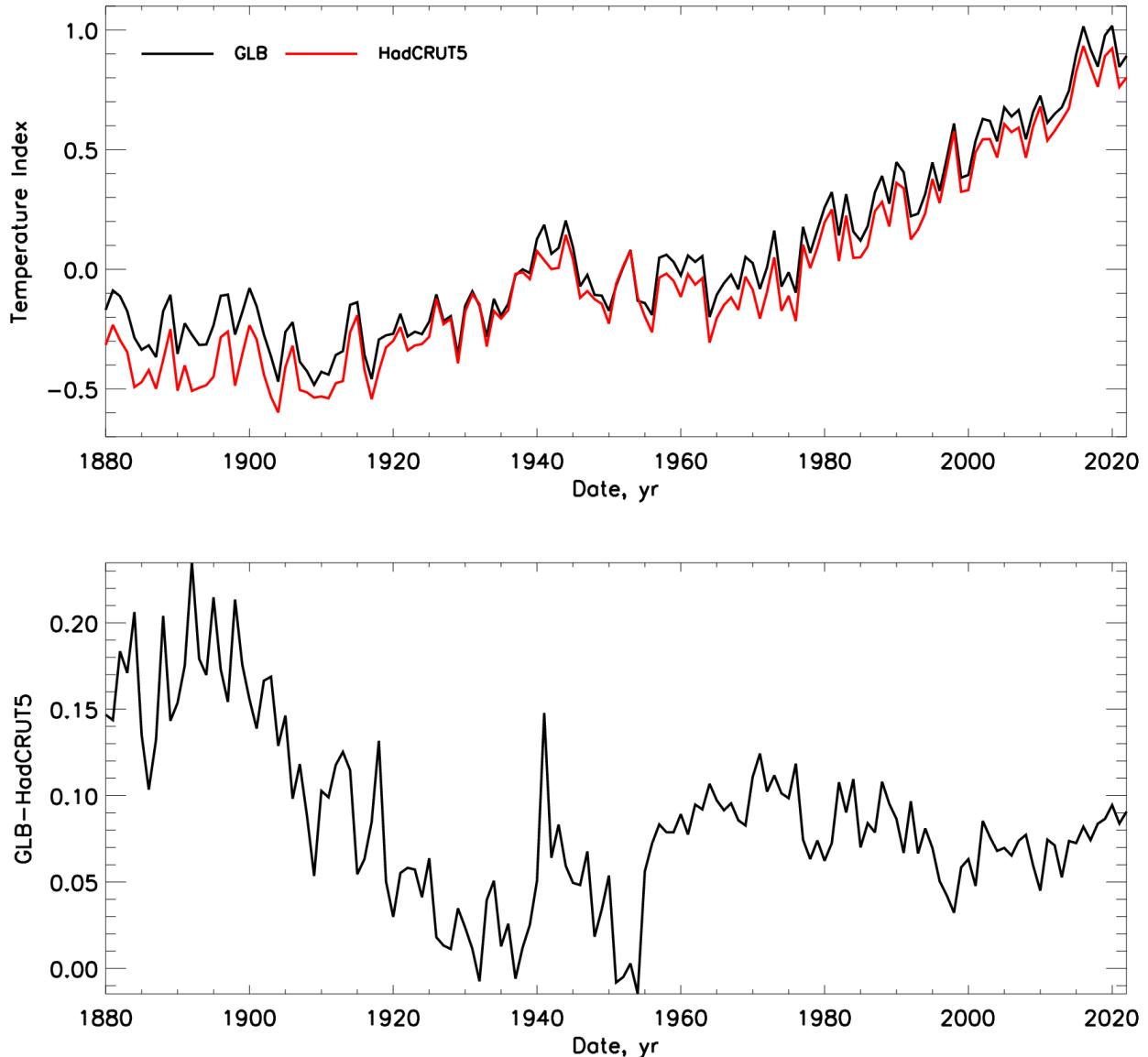
Figure 1: The series of terrestrial temperature variations HadCRUT5 and GLB (see text for more details).

averaged data defined by the red curve, The differences demonstrate the real deviations of the sea level in the given period. In Fig. 3 the similar comparison was carried out of the sea level plots (purple curve) with the temperature variations for the HadCRUTS series (black curve).

The evaluation shows that the sea level is increased by 195 mm during the period from 1870 until 2004 with an averaged speed of growth of 1.7±0.3 mm/year [61]. Although, according to [62], the growth speed of the sea level was 1.7± 0.9 mm/year that led to the global increase of the sea level by 9.2 cm. The satellite data from TOPEX/Poseidon I shows a higher growth speed of the sea level of 3.1 ± 0,7 mm/y ([63, 64]. While [65] reported the average growth speed of 2.3 ranging from 1.6 to 3.1) mm/y during the period of 1971-2018 and 3.7 (3,2-4.2) during the period of 2006-2018.

Indeed, it could be seen that the sea level variations show close similarity, in average, to the temporal variations of the GLB and Had-CRUT temperature curves that confirms findings of the previous studies

[25, 26, 27, 28, 29, 30]. Moreover, the de-trended fluctuation of the sea level reveals a close link between the GLB temperature fluctuations following closely the variations of the temperature curve.

2.3. Ice and snow areas in the Northern and Southern hemispheres

The datasets containing the ice and snow areas in the northern and southern hemispheres including Arctic and Antarctica is taken from the National Snow and Ice Data Center) from 1979 until 2022 accessed on 31/07/2023 $.https : //masie_web.apps.nsidc.org/pub/DATASETS/NOAA/G02135/seaice_analysis/$. The ice and snow cover in different parts of Antarctica is shown in Fig. 4. A comparison of the aggregate areas of the ice and snow cover for both hemispheres (blue curve) with the world sea level ((black curve) is shown in Fig. 5 (top plot) showing a direct comparison of the curves.

In order to detect the finest changes in the world sea level which are usually suppressed on the background of the global level growth we decided to remove this global trend using the averaged sea level animated with a polynomial of the fourth degree as presented by the red line in Fig. 5 (top plot). Then the de-trended plot (black curve) of finest variations of the sea level shown Fig. 5 (bottom plot) is calculated by subtracting the averaged polynomial curve from a real curve of the sea level.

By looking at the plots, it becomes evident that the weather patterns seems to have a very different effect on the Northern and Southern hemispheres. In general, the ice cover in Antarctica demonstrates much smaller variations compared to the ice cover areas in the Northern hemisphere. as shown in Fig. 4. At first, we notice a very interesting feature that in the Southern hemisphere the ice and snow areas were growing until approximately 2013 without any links to solar periods (see Fig. 4 while in the Northern hemisphere from 1986 y there are continuous noticeable decreases of the ice areas, which occur with a period of 10.7 years that is exactly a usual solar activity cycle [43] (see section 3.1.3).

At the second, there is a clear absence of correlation between the variations of the world ocean level (Fig. 5, top plot, black curve) and the variations of the summary ice cover areas in the Northern plus Southern hemispheres (blue curve). This can be understood in terms that only the polar ice cups were considered excluding the ice and snow cover on the continents. Also we did not take into account water expansions under the influence of heat. Although when we include the trend influence shown in Fig. 5 bottom plot, the correlations become more evident by comparing the black and blue curves, especially after 2000.

The estimations of the current loss of mass for the shores of Amudsen glaciers of Pine-Island, Twaits, Smith, Pope and Kohler glacier vary from 1.4 to 2.9 cm per century [18, 19, 20]. The glacier of Pine Island which is the most variable one can lead to the increase of the sea level by 3.5-10 mm during the next 20 years [21, 22, 23].

It is worth mentioning the feature of self-gravitation when increase/decrease of the ice areas leads to a change of sea level and, as a consequence, changes the orientation of the Earth rotation vector that in turn leads to a gravitation anomaly which leads to decrease/increase of the sea level near the glaciers [66, 67].

3. Data analysis

3.1. Wavelet analysis

3.1.1 Method description

Wavelet transform of signals is the spectral analysis method providing a two-dimensional scan of the analysed signal (time and frequency, or period), in which the coordinates of the time and frequency are independent variables [68]. This representation allows one to explore the properties of the signal simultaneously in time and frequency domains. This makes the wavelet analysis an excellent tool for examining the series with time-varying frequency characteristics [68]. By considering the time series in the frequency-time space it is possible to derive dominant periods and their variations in time. The mother wavelet was selected as the Morlet wavelet (the real part of it is damped function of cosine), because with this choice one can obtain a high frequency resolution, which is important for our task.

The power of the wavelet spectra is shown in plots with wavelets by a colour bar plotted next to the wavelet spectrum. The Cone of Influence (COI) marked in the wavelet spectrum by the black dashed line, defines the parts of the spectrum with the essential border effects in the starting and finishing parts of the time series, because of a limited statistical data (boarder effects). Consequently, the results outside the COI are excluded from the further investigation, particularly, in the calculations of the global wavelet spectrum shown by the black curves on the right hand side from the wavelet spectra where we present by the solid black lines the global wavelet spectra integrated over time. The black dashed lines in the global wavelet plots presents 95% confidence interval for the global wavelet spectrum.

3.1.2 Spectral features of the temperature variations

In order to evaluate the spectral properties of the series and to derive the key periods let us apply the Morlet wavelet analysis to both temperature sets with the results presented in Fig. 6 for HadCRUTS (top plot) and GLB (bottom plot) datasets.

The most important feature derived from these two series of terrestrial temperature is a presence of the statistically significant period of 21.4 and 26 years in the GLB series less pronounced at 19.6 years in the HadCRUTS series corresponding to the period of a solar magnetic activity cycle derived in the earlier papers for the summary curve of eigen vectors of the SBMF [43, 52, 53].and the frequency of volcanic eruptions [69].

3.1.3 Spectral features of the ice covers

The wavelet analysis of ice area coverage in Arctic shows (Fig. 7) for the Arctic ice (top plot) and Antarctica ice (bottom plot). It can be observed that the Arctic ice areas change periodically with a period of 10.7 years that is the averaged period of solar activity defined by the averaged sunspot numbers [52, 53].

While Antarctica's ice areas do not reveal this link with the solar activity showing some periods of 5.6 and 15.6 years within the 95% confidence level, possibly, affected by some local events. Curiously, this clear period of 5.6 years which can be linked to a solar activity period reported recently

[70, 71] and interpreted as an important part of defining a solar cycle shape and power. This could reflect the times close to the minima of solar activity when the ice areas are growing.

3.2. Links with solar activity and solar background magnetic field

3.2.1 Solar background magnetic field as a new solar activity proxy

Recently, the Principle Component Analysis was applied to the low-resolution full disk solar background magnetic field (associated with the poloidal magnetic field) measured by the Wilcox Solar Observatory to derive the dominant eigenvalues covering the maximum variance of the data [72, 40, 42] corresponding to the eigenvectors, EVs, or Principal Components (PCs), which came in pairs.

These PCs are considered to be a reflection of the main (dipole) dynamo waves in the solar poloidal magnetic field produced by the dynamo mechanism [40]. The PCs were classified by applying the symbolic regression approach based on the Hamiltonian principle [73] and deriving the mathematical formulae describing the amplitude and phase variations [41, 40].

This summary curve of these two PCs derived for cycles 21-23 and predicted for cycle 24-26 is plotted in Fig. 8 (top plot) also showing the variations of the dominant solar background magnetic field: northern for positive and southern for negative amplitudes. The prediction of the summary curve to cycles 25 and 26 presented in Fig. 8 (top plot) taken from Fig. 2, bottom plot in [40]) shows a noticeable decrease of the predicted average sunspot numbers in cycle 25 to $\approx 80\%$ of that in cycle 24 and in cycle 26 to $\approx 40\%$ that is linked to a reduction of the amplitudes and an increase of phases of the principal components of SBMF. The prediction of the summary curve by thousand years backward and forward presented in Fig.3 [40] revealed the occurrence of grand solar cycle of 350-400 years, reproducing the well-known Maunder, Wolf, Oort, Homeric and many other Grand Solar Minima of the past.

This summary curve was proposed [40] as a new solar activity proxy since the module of the summary curve fits rather closely the averaged sunspot numbers currently used as a solar activity index (Fig. 8, bottom plot). A remarkable resemblance between the modulus summary curve and the curves describing the averaged smoothed sunspot numbers or the averaged sunspot magnetic flux in cycles 21-23 with some small exception for the descending phase of cycle 23, which was later explained by the strongly inflated sunspot numbers used at Locarno observatory [74]. After their correction, the averaged sunspot numbers in cycle 23 fit rather closely the modulus summary curve presented in Fig. 8.

Hence, from the one hand, this modulus summary curve is found to be a good proxy of the traditional solar activity contained in the averaged sunspot numbers. On the other hand, this summary curve is a derivative from the principal components of SBMF with clear mathematical functionalities representing at the same time the real physical processes - poloidal field dynamo waves - generated by the solar dynamo [40]. Recently, the other PCs, or eigen vectors of SBMF derived from the SBMF data for four cycle 21-24 supposedly produced by quadruple, sextuple and octuple mag-

netic sources are shown linked to various flare activity indices in soft X-ray and radio emission [42].

The suggestion of usage of the summary curve of two eigen vectors, or principle components of the solar background magnetic field as a new proxy of solar activity has been recently supported by other predictions of the solar activity in cycle 25 [75, 76] obtained from the same solar magnetic field components measured from the same WSO magnetic synoptic maps as those reported earlier [41, 40].

3.2.2 Key periods in the terrestrial temperature and ocean level variations

In this section we explore the links between the variations of solar activity and solar background magnetic field. and the world sea level (Fig.9, top plot), the aggravated (total) ice ares in both hemispheres (Fig.9, bottom plot) and terrestrial temperature (Fig. 10) variations occurred in the past two centuries.

It can be observed that there is clearly present a dominant 21.4-years period of variations of the world sea level shown in Fig.9, top plot and not so recognisable tendency of the temperature variations either from SBMF (top plot) or the sunspot index of solar activity (bottom plot) shown in Fig.10. The agreement between the periods of the sea lveel curves and the eigen vectors in the summary curve of SBMF confirm the conclusions about the similar period detected in the link between the eigen vectors of SBMF and the frequency of volcanic eruptions [69]. It has been shown that the volcanic eruptions occur mainly during the maximum phases of the doubled solar cycles of 22 years of SBMF when the eigen vector of the summary curve of SBMF has a southern polarity. This case was in cycle 24, and it will be approaching again during cycle 26. This will coincide when the grand solar minimum in solar activity predicted for the duration of 2020-2053 [40, 45].

We also established a rather high positive correlation of the areas covered by the ice in the both hemispheres and the SBMF ((Fig.9, top plot) showing the increase of the ice areas when the summary curve of SBMF has the southern polarity and a decrease of the ice areas when it has the northern polarity. The weak but visible link is detected between the terrestrial temperature with the summary curve of SBMF in Fig.10, top plot, while there is no clear link is seen with the solar activity defined by sunspot numbers in Fig.10, bottom plot. This absence of the link can be related to the difficulties defining the averaged sunspot numbers which wee described in our previous paper [43].

3.3. Links of the terrestrial temperature and solar irradiance induced by inertial motion

Solar inertial motion is a rotation of the Sun about the barycentre of planetary orbits caused by the gravitation of large planets of the solar system (Jupiter, Saturn, Neptune and Uranus) [77, 78, 79]. The methodology for the calculation of total solar irradiance (TSI) using inverse squares of the distance between the Sun and Earth is described in the book chapter by [51], which also provided the plots of solar irradiance variations in the two millennia 600-2600.

The TSI results calculated for March-August -September of the relevant years in the past two centuries are plotted above the terrestrial temperature curve as shown in Fig. 11 (top plot) while the TSI results obtained for the SIM during the whole year are shown in Fig. 11 (bottom plot).

It can be seen that the sum of all TSI in W/m^2 deposited to the Earth daily during the period when the Sun is closest to the Earth's orbit (March-July) grows with every coming year of this millennium because the Sun moves closer and closer to the Earth orbit and to other planetary orbits. This is caused by the solar inertial motion shifting the Sun from the ellipse focus towards the Northern hemisphere spring equinox position. It can be seen that the total solar irradiance magnitudes calculated for the spring-summer months when the Sun is closest to the Earth orbit follow rather closely the temperature trend.

The sharp increase of the terrestrial temperature after 2010 can be reasonably explained by the temperature measurements on the surface instead of two meters above it used in previous years and carrying the measurements in urban areas which are higher by default because of asphalt coverage of the surface [80, 81]. However, if the sum of TSI calculated for the whole year, the deposited solar radiation has a wide variation in magnitudes imposed by the smaller SIM effects remaining though nearly a constant wide strip over the time of two centuries. Not least contribution to the increase of the temperature can come also from the increase of solar activity in cycle 25, which approached its maximum in 2022-2025.

This growth of solar irradiance during spring and summer months caused by the Sun moving closer to the Earth orbit is evidently reflected in the temperature trend measured by the NASA stations, which seems to miss the temperature measurements in the same locations during the other months September - February when TSI and, consequently, the temperature, drops much lower than expected for a normal Sun's position in the focus of the elliptic orbit of the Earth and other planets. This is a very important finding because of a close correlation of the this temperature curve with the ocean level shown in Fig. 3 as it indicates that the extra-heating provided by the Sun at the times, when it is closer to the Earth orbit, is consumed by the ocean and is likely to be processed over the next months or years.

The fact that the ocean level correlates with the spring-summer TSI magnitudes, which is not considered when producing the solar forcing for the terrestrial temperature models [3] is likely to create the discrepancy between the solar heating function used in the current temperature models. Besides any increases of the terrestrial temperature caused by the temperature measurements in urban conditions where temperature by default is higher [80, 81]., there is additional solar heating caused by solar orbital motion induced by the gravitation of large planets.

In the other words, the solar heating applied in the IPCC models uses the TSI magnitudes averaged over the annual Earth orbit while the real temperature measurements they use to interpret are likely too be carried only during the spring-summer periods when the Sun's input is maximal because it is closest to the Earth orbit. What is also important that only the current temperature measurements made in March–August are closely linked to the ocean level as discovered in this study, thus affecting the exchange between the ocean and atmosphere.

4. Discussion and conclusions

In this study we explored the links of the terrestrial temperature measurements, the world sea level and ice area in both hemispheres with a) the solar activity indices expressed through the averaged sunspot numbers, the summary curve of two largest eigen vectors of the solar background magnetic field and b) the changes of Sun-Earth distances caused by solar inertial motion imposed by the gravitation of large planets of the solar system.

We explored the two sets of the terrestrial temperature variations obtained since 1850 using the wavelet analysis and detected in the GLB datasets a clear period of 21.4 and 36 years, while in the HadCRUTS dataset only weaker indication of the period of about 19.6 years. This 21.4 y period is clearly associated with the variations of solar activity defined by the eigen vectors of the solar background magnetic field (SBMF) [52, 53]. The similar period of 21.4 years was also reported previously in the frequency of volcanic eruptions [69].

It was established that the sea level curve showed rather close similarity, in average, to the temporal variations of the temperature curves that was also reported by the other studies [25, 26, 27, 28, 29, 30]. A comparison shows that there is clearly present a dominant 21.4-year period of variations of the world sea level linked to the summary curve of the largest eigen vectors of SBMF [40] coinciding with the period of 21.4 years detected in the GLB temperature variations, while there is no recognisable tendency of the temperature variations from the sunspot index of solar activity.

Although, the weather patterns seem to affect the Northern and Southern hemispheres very differently. For example, the ice cover in Antarctica demonstrates much smaller variations compared to the ice cover areas in the Northern hemisphere. Wavelet analysis shows that in the Southern hemisphere the ice and snow areas were growing until approximately 2013 without any links to the solar periods while in the Northern hemisphere there is continuous noticeable decrease of the ice areas, which occurs periodically with a period of 10.7 years that is a usual solar cycle defined by sunspots [43]. There is a clear absence of correlation between the curves of the sea level and the ice areas meaning that the ice areas are not also dependent on the terrestrial temperature which is shown linked to the sea levels.

Also it was established that the Arctic ice area changes periodically with a period of 10.7 years that is the averaged period of solar activity defined by averaged sunspot numbers. While Antarctica's ice areas do not reveal this link with the solar activity showing some periods of 5.6 and 15.6 years within the 95% confidence level, possibly, affected by some local events.

Most interesting results, though, are found from the comparison of the temperature and sea level curves with the total solar irradiance variations caused by solar inertial motion induced by the gravitation of large planets on the noticeable shift of the Sun from the focus of the elliptic orbits. The TSI during the period when the Sun is closest to the Earth's orbit (March-July) grows with every coming year of this millennium because the Sun moves closer and closer to the Earth orbit and to other planetary orbits. The annual variations of TSI have a wider dispersion but more steady TSI curve without a very sharp increase in the last two centuries. This steady TSI trend is used by the IPCC as the current solar forcing.

This TSI growth is evidently reflected in the temperature trend measured by the NASA stations, and in the sea level variations via its link with the temperature. This reflects the fact that the solar forcing works during the spring-summer months depositing the solar energy into the ocean and seas, which process it in the later months. Not speaking about the problems of how the temperature curve is obtained from the measurements in the urban areas or by taking only the measurements in the same location during the hottest months and underestimating the temperature measurements in the colder months. Definitely, the solar forcing function has to be amended to reflect this deposition of solar energy during the spring-summer months, which follows closely the temperature variation curve and the sea level curve linked to the temperature variations.

This means that the solar energy deposition to Earth is much higher in these spring-summer months and this deposition occurring in the Southern hemisphere in March-April and the southern part of the northern hemisphere in May-August, which is mostly covered by the world oceans. This explains a close correlation between the temperature and sea level detected in this study and the increase of the sea level during the summer months. It turns out that the sea water has to play a very important role in transferring this solar energy into the terrestrial atmosphere via the water vapour [56, 57].

The sea level variations are shown to be linked to solar magnetic field variations, or more precisely, to the summary eigen vectors of SBMF varying with a period of 21.4 years and having maximal sea level when the summary curve has the southern polarity and the minimal one when the summary curve polarity is northern. These variations are similar to those detected for the frequency of volcanic eruptions with a period f 21.4 years with maximal number of eruptions occurring during the maxima during the cycles when the summary curve has the southern polarity and minima during the cycles when the summary curve has the northern polarity.

In summary, we have presented a growing evidence that the terrestrial temperature, sea level and ice coverage variations on Earth are linked to the variations of solar magnetic field, or its summary curve of two largest eigen vectors reflecting the cycles of solar activity, and the orbital motion of the Earth and solar inertial motion of the Sun caused by the gravitation of large planets of the solar system. The combined effect of the solar heating from solar activity and orbital motion imposing the variable Sun-Earth distances, approaches its maximum magnitudes during March-July of each year causing substantial heating of the Earth's atmosphere and sea that will keep increasing with every year of the current millennium (1600-2600) following the trajectory of solar inertial motion and magnetic polarity of the summary curve of the SBMF.

5. Acknowledgments

Author contributions statement

V.Z. formulated the problem, suggested the datasets to consider, did calculations and analysis of the eigen vectors sbmf and TSI for different Sun-Earth distances. I.V. gathered and processed the temperature, ice area and sea level data, analysed them with the wavelet tool. V.Z. and I.V. compared and analysed the results, wrote and reviewed the manuscript.

Additional information

The authors do not have any competing financial interests.

References

[1] S.-I. Akasofu, "On the recovery from the little ice age," *Natural Science*, vol. 2, pp. 1211–1224, Nov. 2010.

[2] J. Hansen, R. Ruedy, M. Sato, and K. Lo, "Global Surface Temperature Change," *Reviews of Geophysics*, vol. 48, p. RG4004, Dec. 2010.

[3] j. C. P. S. B. IPCC, title = 'Contribution of Working Group I to the Fifth Assessment Report of the Intergovernmental Panel on Climate Change" 04 2023.

[4] S. Y. Yim, B. Wang, and X. Wu, "A comparison of regional monsoon variability using monsoon indices," *Climate Dyn.*, vol. 43, pp. 1423–1437, jun 2013.

[5] K. E. Trenberth and T. J. Hoar, "El Niño and climate change," *Geophys. Res. Let.*, vol. 24, pp. 3057–3060, dec 1997.

[6] K. Ashok, Z. Guan, and T. Yamagata, "Impact of the Indian Ocean dipole on the relationship between the Indian monsoon rainfall and ENSO," *Geophysics Research Letters*, vol. 28, pp. 4499–4502, Dec. 2001.

[7] K. Ashok and T. Yamagata, "Climate change: The El Niño with a difference," *Nature*, vol. 461, pp. 481–484, Sept. 2009.

[8] S.-W. Yeh, J.-S. Kug, B. Dewitte, M.-H. Kwon, B. P. Kirtman, and F.-F. Jin, "El Niño in a changing climate," *Nature*, vol. 462, p. 674, Dec. 2009.

[9] I. Roy, T. Asikainen, V. Maliniemi, and K. Mursula, "Comparing the influence of sunspot activity and geomagnetic activity on winter surface climate," *Journal of Atmospheric and Solar-Terrestrial Physics*, vol. 149, pp. 167–179, Nov. 2016.

[10] M. J. McPhaden and D. Zhang, "Pacific Ocean circulation rebounds," *Geophysics Research Letters*, vol. 31, p. L18301, Sept. 2004.

[11] G. A. Vecchi and B. J. Soden, "Effect of remote sea surface temperature change on tropical cyclone potential intensity," *Nature*, vol. 450, pp. 1066–1070, Dec. 2007.

[12] S. Minobe, "Spatio-temporal structure of the pentadecadal variability over the North Pacific," *Progress in Oceanography*, vol. 47, pp. 381–408, oct 2000.

[13] N. A. Bond, J. E. Overland, M. Spillane, and P. Stabeno, "Recent shifts in the state of the North Pacific," *Geophys. Res. Let.*, vol. 30, p. 2183, Dec. 2003.

[14] A. R. Simms, M. J. Bentley, L. M. Simkins, J. Zurbuchen, L. C. Reynolds, R. DeWitt, and E. R. Thomas, "Evidence for a little ice age glacial advance within the antarctic peninsula examples from glacially-overrun raised beaches," *Quaternary Science Reviews*, vol. 271, p. 107195, 2021.

[15] J. C. Moore, A. Grinsted, T. Zwinger, and S. Jevrejeva, "Semiempirical and process-based global sea level projections," *Reviews of Geophysics*, vol. 51, pp. 484–522, Sept. 2013.

[16] J. Fyke, O. Sergienko, M. Löfverström, S. Price, and J. T. M. Lenaerts, "An Overview of Interactions and Feedbacks Between Ice Sheets and the Earth System," *Reviews of Geophysics*, vol. 56, pp. 361–408, June 2018.

[17] J. Turner, A. Orr, G. H. Gudmundsson, A. Jenkins, R. G. Bingham, C.-D. Hillenbrand, and T. J. Bracegirdle, "Atmosphere-ocean-ice interactions in the Amundsen Sea Embayment, West Antarctica," *Reviews of Geophysics*, vol. 55, pp. 235–276, Mar. 2017.

[18] H. D. Pritchard, R. J. Arthern, D. G. Vaughan, and L. A. Edwards, "Extensive dynamic thinning on the margins of the Greenland and Antarctic ice sheets," *Nature*, vol. 461, pp. 971–975, Oct. 2009.

[19] E. Rignot, J. L. Bamber, M. R. van den Broeke, C. Davis, Y. Li, W. J. van de Berg, and E. van Meijgaard, "Recent Antarctic ice mass loss from radar interferometry and regional climate modelling," *Nature Geoscience*, vol. 1, pp. 106–110, Feb. 2008.

[20] I. Joughin, B. E. Smith, and D. M. Holland, "Sensitivity of 21st century sea level to ocean-induced thinning of Pine Island Glacier, Antarctica," *Geophysics Research Letters*, vol. 37, p. L20502, Oct. 2010.

[21] L. Favier, G. Durand, S. L. Cornford, G. H. Gudmundsson, O. Gagliardini, F. Gillet-Chaulet, T. Zwinger, A. J. Payne, and A. M. Le Brocq, "Retreat of Pine Island Glacier controlled by marine ice-sheet instability," *Nature Climate Change*, vol. 4, pp. 117–121, Feb. 2014.

[22] J. W. Park, N. Gourmelen, A. Shepherd, S. W. Kim, D. G. Vaughan, and D. J. Wingham, "Sustained retreat of the Pine Island Glacier," *Geophysics Research Letters*, vol. 40, pp. 2137–2142, May 2013.

[23] D. J. Wingham, D. W. Wallis, and A. Shepherd, "Spatial and temporal evolution of Pine Island Glacier thinning, 1995-2006," *Geophysics Research Letters*, vol. 36, p. L17501, Sept. 2009.

[24] A. Cazenave, H.-B. Dieng, B. Meyssignac, K. von Schuckmann, B. Decharme, and E. Berthier, "The rate of sea-level rise," *Nature Climate Change*, vol. 4, pp. 358–361, May 2014.

[25] S. Rahmstorf, "A Semi-Empirical Approach to Projecting Future Sea-Level Rise," *Science*, vol. 315, p. 368, Jan. 2007.

[26] R. S. Nerem, B. D. Beckley, J. T. Fasullo, B. D. Hamlington, D. Masters, and G. T. Mitchum, "Climate-change-driven accelerated sea-level rise detected in the altimeter era," *Proceedings of the National Academy of Science*, vol. 115, pp. 2022–2025, Mar. 2018.

[27] H. V. Storch, E. Zorita, and J. F. González-Rouco, "Relationship between global mean sea-level and global mean temperature in a climate simulation of the past millennium," *Ocean Dynamics*, vol. 58, pp. 227–236, Nov. 2008.

[28] A. Grinsted, J. C. Moore, and S. Jevrejeva, "Reconstructing sea level from paleo and projected temperatures 200 to 2100 ad," *Climate Dynamics*, vol. 34, pp. 461–472, Mar. 2010.

[29] M. Vermeer and S. Rahmstorf, "From the Cover: Global sea level linked to global temperature," *Proceedings of the National Academy of Science*, vol. 106, pp. 21527–21532, Dec. 2009.

[30] G. Sannino, A. Carillo, R. Iacono, E. Napolitano, M. Palma, G. Pisacane, and M. Struglia, "Modelling present and future climate in the Mediterranean Sea: a focus on sea-level change," *Climate Dynamics*, vol. 59, pp. 357–391, July 2022.

[31] K. Ashok, S. K. Behera, S. A. Rao, H. Weng, and T. Yamagata, "El Niño Modoki and its possible teleconnection," *Journal of Geophysical Research (Oceans)*, vol. 112, p. C11007, Nov. 2007.

[32] Y.-P. Chang, M.-T. Chen, Y. Yokoyama, H. Matsuzaki, W. G. Thompson, S.-J. Kao, and H. Kawahata, "Monsoon hydrography and productivity changes in the East China Sea during the past 100,000 years: Okinawa Trough evidence (MD012404)," *Paleoceanography*, vol. 24, p. PA3208, Sept. 2009.

[33] T. Hao, X. Liu, J. Ogg, Z. Liang, R. Xiang, X. Zhang, D. Zhang, C. Zhang, Q. Liu, and X. Li, "Intensified episodes of East Asian Winter Monsoon during the middle through late Holocene driven by North Atlantic cooling events: High-resolution lignin records from the South Yellow Sea, China," *Earth and Planetary Science Letters*, vol. 479, pp. 144–155, Dec. 2017.

[34] I. Roy and J. D. Haigh, "Solar cycle signals in sea level pressure and sea surface temperature," *Atmospheric Chemistry & Physics*, vol. 10, pp. 3147–3153, Mar. 2010.

[35] P. Christoforou and S. Hameed, "Solar cycle and the Pacific 'centers of action'," *Geophysics Research Letters*, vol. 24, pp. 293–296, Feb. 1997.

[36] H. van Loon and G. A. Meehl, "The response in the Pacific to the sun's decadal peaks and contrasts to cold events in the Southern Oscillation," *Journal of Atmospheric and Solar-Terrestrial Physics*, vol. 70, pp. 1046–1055, may 2008.

[37] L. Oman, A. Robock, and G. Stenchikov, "Comparing the Climatic Impact from Low Latitude versus High Latitude Volcanic Eruptions," in *AGU Fall Meeting Abstracts*, vol. 2003, pp. A41D–0725, Dec. 2003.

[38] J. Emile-Geay, R. Seager, M. A. Cane, E. R. Cook, and G. H. Haug, "Volcanoes and ENSO over the Past Millennium," *Journal of Climate*, vol. 21, p. 3134, Jan. 2008.

[39] W. B. White, J. Lean, D. R. Cayan, and M. D. Dettinger, "Response of global upper ocean temperature to changing solar irradiance," *Journal of Geophysics Research*, vol. 102, pp. 3255–3266, Feb. 1997.

[40] V. V. Zharkova, S. J. Shepherd, E. Popova, and S. I. Zharkov, "Heartbeat of the Sun from Principal Component Analysis and prediction of solar activity on a millenium timescale," *Scientific Reports*, vol. 5, p. 15689, Oct. 2015.

[41] S. J. Shepherd, S. I. Zharkov, and V. V. Zharkova, "Prediction of Solar Activity from Solar Background Magnetic Field Variations in Cycles 21-23," *Astrophysical J.*, vol. 795, p. 46, Nov. 2014.

[42] V. V. Zharkova and S. J. Shepherd, "Eigen vectors of solar magnetic field in cycles 21-24 and their links to solar activity indices," *Monthly Notices of Royal Astron.Soc.*, vol. 512, pp. 5085–5099, Mar. 2022.

[43] V. V. Zharkova, I. Vasilieva, E. Popova, and S. J. Shepherd, "Comparison of solar activity proxies: eigenvectors versus averaged sunspot numbers," *Monthly Notices Royal Astron. Soc.*, vol. 521, pp. 6247–6265, June 2023.

[44] J. A. Eddy, "The Maunder Minimum," *Science*, vol. 192, pp. 1189–1202, June 1976.

[45] V. Zharkova, "Modern grand solar minimum will lead to terrestrial cooling," *Editorial paper, Temperature*, vol. 7, no. 3, pp. 217–222, 2020.

[46] J. Lean, J. Beer, and R. Bradley, "Reconstruction of solar irradiance since 1610: Implications for climate change," *Geophys. Res. Letters*, vol. 22, pp. 3195–3198, Jan. 1995.

[47] D. J. Easterbrook, *Evidence-based Climate Science.* Elsevier, May 2016.

[48] D. E. Parker, P. D. Jones, C. K. Folland, and A. Bevan, "Interdecadal changes of surface temperature since the late nineteenth century," *J. Geophys. Research: Atmospheres*, vol. 99, no. D7, pp. 14373–14399, 1994.

[49] M. Lockwood, R. Stamper, and M. N. Wild, "A doubling of the Sun's coronal magnetic field during the past 100 years," *Nature*, vol. 399, pp. 437–439, June 1999.

[50] V. V. Zharkova, S. J. Shepherd, S. I. Zharkov, and E. Popova, "RETRACTED ARTICLE: Oscillations of the baseline of solar magnetic field and solar irradiance on a millennial timescale," *Scientific Reports*, vol. 9, p. 9197, June 2019.

[51] V. Zharkova, "Millennial Oscillations of Solar Irradiance and Magnetic Field in 600-2600," *chapter in a book "Solar system planets and exoplanets"*, p. 30 pp., Mar. 2021.

[52] V. V. Zharkova, I. Vasilieva, S. Shepherd, and E. Popova, "Periodicities of solar activity and solar radiation derived from observations and their links with the terrestrial environment," *arXiv e-prints*, p. arXiv:2301.07480, Jan. 2023.

[53] V. V. Zharkova, I. Vasilieva, S. Shepherd, and E. Popova, "Periodicities of solar activity and solar radiation derived from observations and their links with the terrestrial environment," *Natural Science*, vol. 15, p. 56 pp, Mar. 2023.

[54] F. Steinhilber, J. Beer, and C. Fröhlich, "Total solar irradiance during the Holocene," *Geophys. Res. Letters*, vol. 36, p. L19704, Oct. 2009.

[55] F. Steinhilber, J. A. Abreu, J. Beer, I. Brunner, M. Christl, H. Fischer, U. Heikkila, P. W. Kubik, M. Mann, K. G. McCracken, H. Miller, H. Miyahara, H. Oerter, and F. Wilhelms, "9,400 years of cosmic radiation and solar activity from ice cores and tree rings," *Proceedings of the National Academy of Science*, vol. 109, pp. 5967–5971, Apr. 2012.

[56] M. L. Salby, E. A. Titova, and L. Deschamps, "Changes of the Antarctic ozone hole: Controlling mechanisms, seasonal predictability, and evolution," *Journal of Geophysical Research (Atmospheres)*, vol. 117, p. D10111, May 2012.

[57] I. Roy, "Addressing on abrupt global warming, warming trend slowdown and related features in recent decades," *Frontiers in Earth Science*, vol. 6, p. 136, Sept. 2018.

[58] D. Koutsoyiannis, C. Onof, Z. Kundzewicz, and A. Christofides, "On Hens, Eggs, Temperatures and CO2: Causal Links in EarthÕs Atmosphere," *MDPI Sci*, vol. 5, p. 35, sep 2023.

[59] N. J. L. Lenssen, G. A. Schmidt, J. E. Hansen, M. J. Menne, A. Persin, R. Ruedy, and D. Zyss, "Improvements in the gistemp uncertainty model," *Journal of Geophysical Research: Atmospheres*, vol. 124, no. 12, pp. 6307–6326, 2019.

[60] J. Church and N. White, "Sea-level rise from the late 19th to the early 21st century," *Surveys in Geophysics*, vol. 32, pp. 585–602, 09 2011.

[61] J. A. Church and N. J. White, "A 20th century acceleration in global sea-level rise. geophys res lett 33: L01602," *Geophysical Research Letters*, vol. 33, p. L01602, 01 2006.

[62] S. Holgate, "Evidence for enhanced coastal sea level rise during the 1990s," *Geophysical Research Letters - GEOPHYS RES LETT*, vol. 31, 04 2004.

[63] A. Cazenave and R. Nerem, "Present-day sea level change: Observations and causes," *Rev. Geophys*, vol. 42, 09 2004.

[64] E. W. Leuliette, R. S. Nerem, and G. T. Mitchum, "Calibration of topex/poseidon and jason altimeter data to construct a continuous record of mean sea level change," *Marine Geodesy*, vol. 27, no. 1-2, pp. 79–94, 2004.

[65] B. Fox-Kemper, H. Hewitt, C. Xiao, G. Aethalgeirsdottir, S. Drijfhout, T. Edwards, N. Golledge, M. Hemer, R. Kopp, G. Krinner, A. Mix, D. Notz, S. Nowicki, I. Nurhati, L. Ruiz, J.-B. Sallée, A. Slangen, and Y. Yu, *Ocean, Cryosphere and Sea Level Chang.* Cambridge, United Kingdom and New York, NY, USA: Cambridge University Press, 2021.

[66] J. A. Clark, "Future sea-level changes due to West Antarctic ice sheet fluctuations," *Nature*, vol. 269, pp. 206–209, Sept. 1977.

[67] N. Gomez, J. X. Mitrovica, M. E. Tamisiea, and P. U. Clark, "A new projection of sea level change in response to collapse of marine sectors of the Antarctic Ice Sheet," *Geophysical Journal International*, vol. 180, pp. 623–634, Feb. 2010.

[68] C. Torrence and G. P. Compo, "A practical guide to wavelet analysis," *Bull. of American Meteorological Society*, vol. 79, pp. 61–78, Mar. 1998.

[69] I. Vasilieva and V. Zharkova, "Terrestrial volcanic eruptions and their association with solar activity," *Global Journal of Science Frontier Research*, vol. 23, p. 22pp, Mar. 2023.

[70] V. M. Velasco Herrera, W. Soon, and D. R. Legates, "Does Machine Learning reconstruct missing sunspots and forecast a new solar minimum?," *Advances in Space Research*, vol. 68, pp. 1485–1501, Aug. 2021.

[71] J. L. Le Mouël, F. Lopes, and V. Courtillot, "Characteristic Time Scales of Decadal to Centennial Changes in Global Surface Temperatures Over the Past 150 Years," *Earth and Space Science*, vol. 7, p. e00671, Apr. 2020.

[72] V. V. Zharkova, S. J. Shepherd, and S. I. Zharkov, "Principal component analysis of background and sunspot magnetic field variations during solar cycles 21-23," *Monthly Notices of Royal Astron.Soc.*, vol. 424, pp. 2943–2953, Aug. 2012.

[73] M. Schmidt and H. Lipson, "Distilling free-form natural laws from experimental data," *Science*, vol. 324, pp. 81–85, Apr. 2009.

[74] F. Clette, L. Svalgaard, J. M. Vaquero, and E. W. Cliver, "Revisiting the Sunspot Number. A 400-Year Perspective on the Solar Cycle," *Space Science Reviews*, vol. 186, pp. 35–103, Dec. 2014.

[75] I. N. Kitiashvili, "Application of Synoptic Magnetograms to Global Solar Activity Forecast," *Astrophysical J.*, vol. 890, p. 36, Feb. 2020.

[76] V. N. Obridko, D. D. Sokoloff, V. V. Pipin, A. S. Shibalvaa, and I. M. Livshits, "Zonal harmonics of solar magnetic field for solar cycle forecast," *Monthly Notices of Royal Astr. Soc*, pp. 4990–5000, Apr. 2021.

[77] I. Charvátová, "Can origin of the 2400-year cycle of solar activity be caused by solar inertial motion?," *Annales Geophysicae*, vol. 18, pp. 399–405, Apr. 2000.

[78] M. Paluš, J. Kurths, U. Schwarz, N. Seehafer, D. Novotná, and I. Charvátová, "The solar activity cycle is weakly synchronized with the solar inertial motion," *Physics Letters A*, vol. 365, pp. 421–428, June 2007.

[79] A. S. Perminov and E. D. Kuznetsov, "Orbital Evolution of the Sun-Jupiter-Saturn-Uranus-Neptune Four-Planet System on Long-Time Scales," *Solar System Research*, vol. 52, pp. 241–259, May 2018.

[80] R. Connolly, W. Soon, M. Connolly, S. Baliunas, J. Berglund, C. J. Butler, R. Gustavo Cionco, A. G. Elias, V. M. Fedorov, H. Harde, G. W. Henry, D. V. Hoyt, O. Humlum, D. R. Legates, N. Scafetta, J.-E. Solheim, L. Szarka, V. M. Velasco Herrera, H. Yan, and W. Zhang, "Challenges in the Detection and Attribution of Northern Hemisphere Surface Temperature Trends Since 1850," *Research in Astronomy and Astrophysics*, vol. 23, p. 105015, Oct. 2023.

[81] W. Soon, R. Connolly, M. Connolly, S.-I. Akasofu, S. Baliunas, J. Berglund, A. Bianchini, W. M. Briggs, C. J. Butler, R. G. Cionco, M. Crok, A. G. Elias, V. M. Fedorov, F. Gervais, H. Harde, G. W. Henry, D. V. Hoyt, O. Humlum, D. R. Legates, A. R. Lupo, S. Maruyama, P. Moore, M. Ogurtsov, C. ÓhAiseadha, M. J. Oliveira, S.-S. Park, S. Qiu, G. Quinn, N. Scafetta, J.-E. Solheim, J. Steele, L. Szarka, H. L. Tanaka, M. K. Taylor, F. Vahrenholt, V. M. Velasco Herrera, and W. Zhang, "The Detection and Attribution of Northern Hemisphere Land Surface Warming (1850-2018) in Terms of Human and Natural Factors: Challenges of Inadequate Data," *Climate*, vol. 11, p. 179, Aug. 2023.
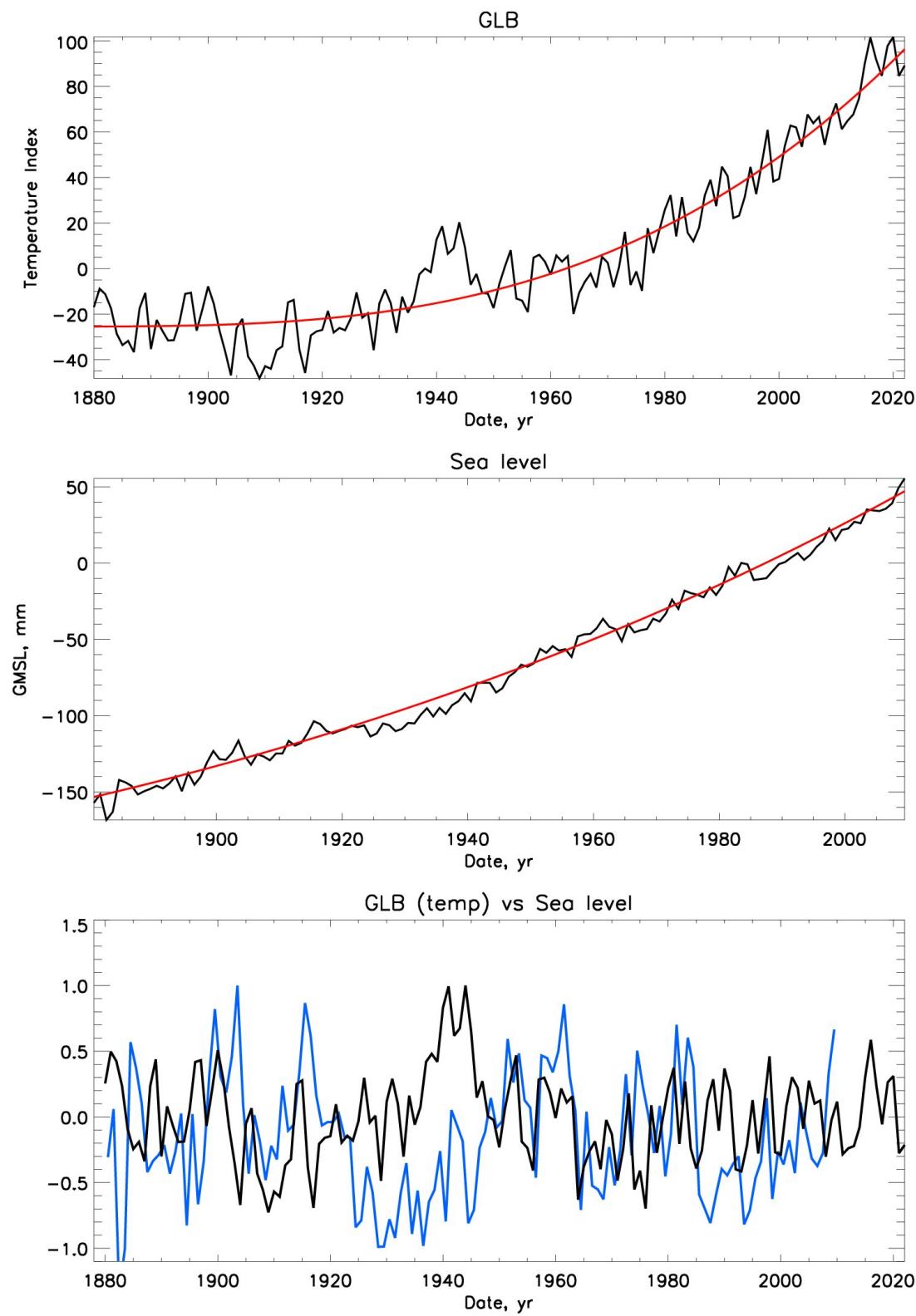
Figure 2: Top plot: The GLB temperature variations (black line) and averaged variations presented by a polynomial of the 4th degree (red curve). Middle plot: the sea level variations (black curve) and averaged curve presented by a polynomial of the 4th degree (red curve). Bottom plot: A comparison of the GLB temperature variations (black curve) with the de-trended sea level variations (blue curve) calculated by subtracting the averaged sea level from the real sea level curve, thus revealing the finest deviation of the sea levels.
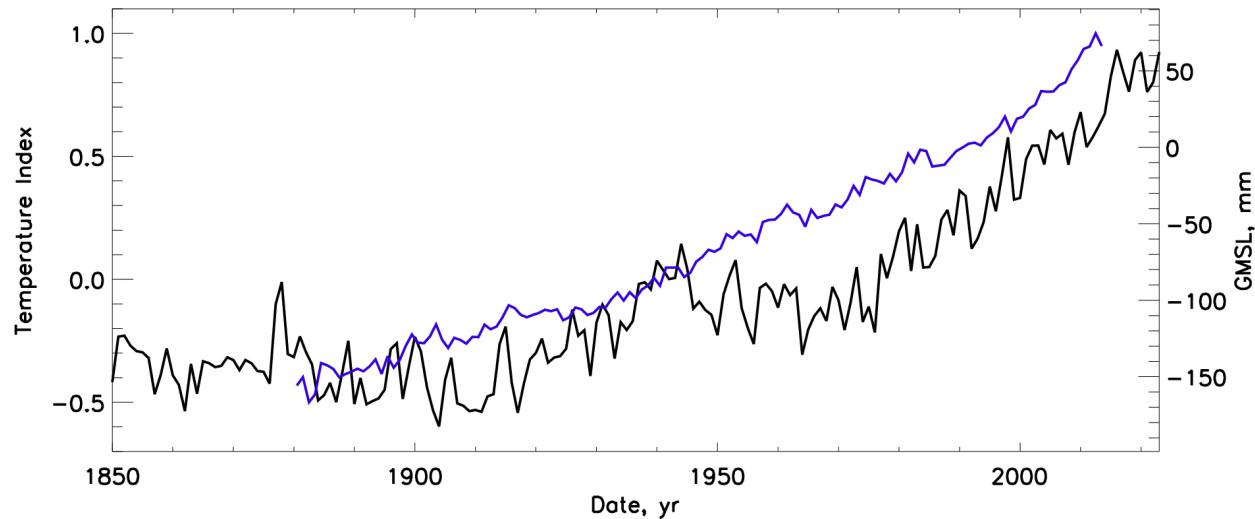
Figure 3: The sea level variations (blue curve) versus the terrestrial temperature dataset HadCRUT (black curve).
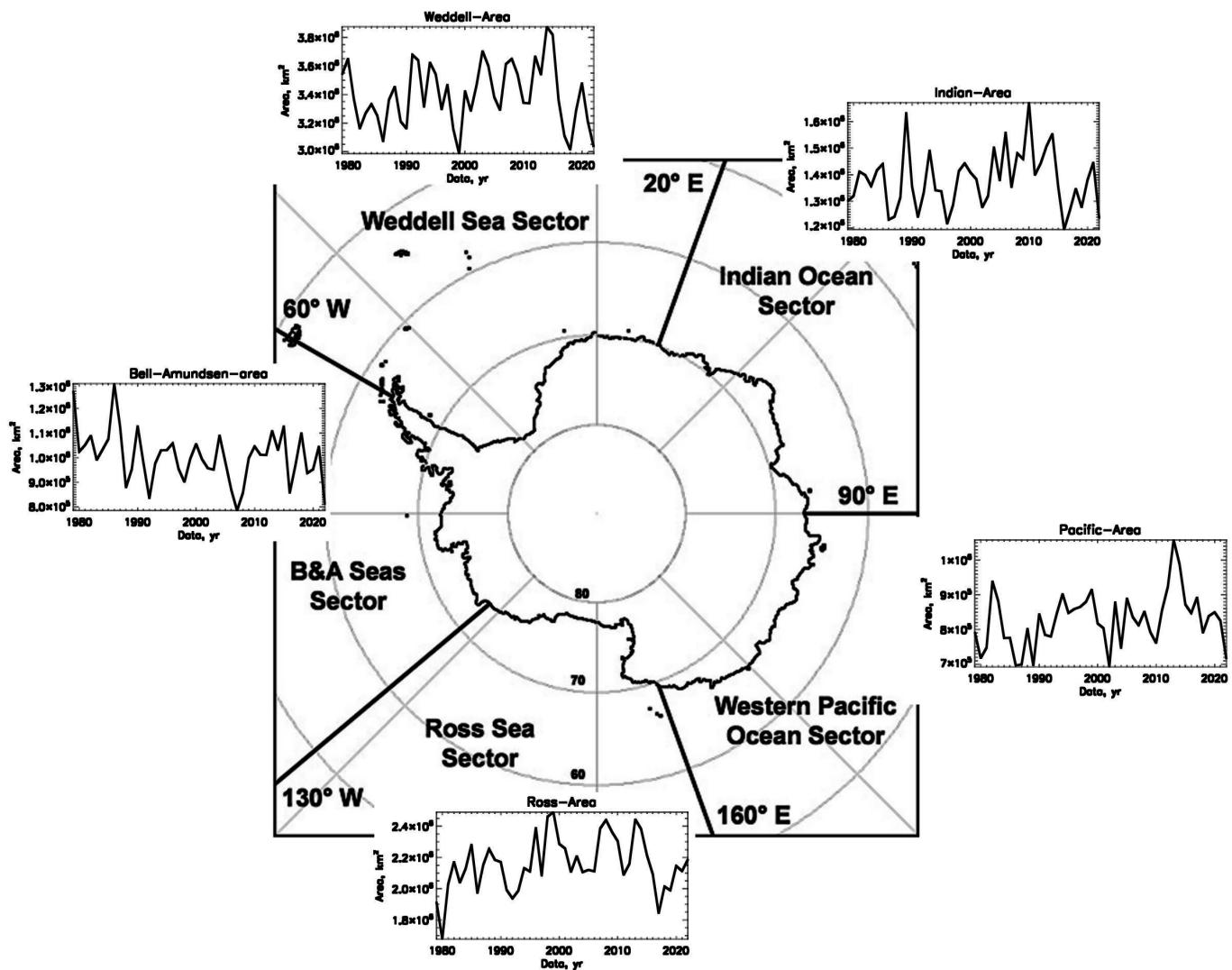
Figure 4: Change of the ice areas in different parts of Antarctica.
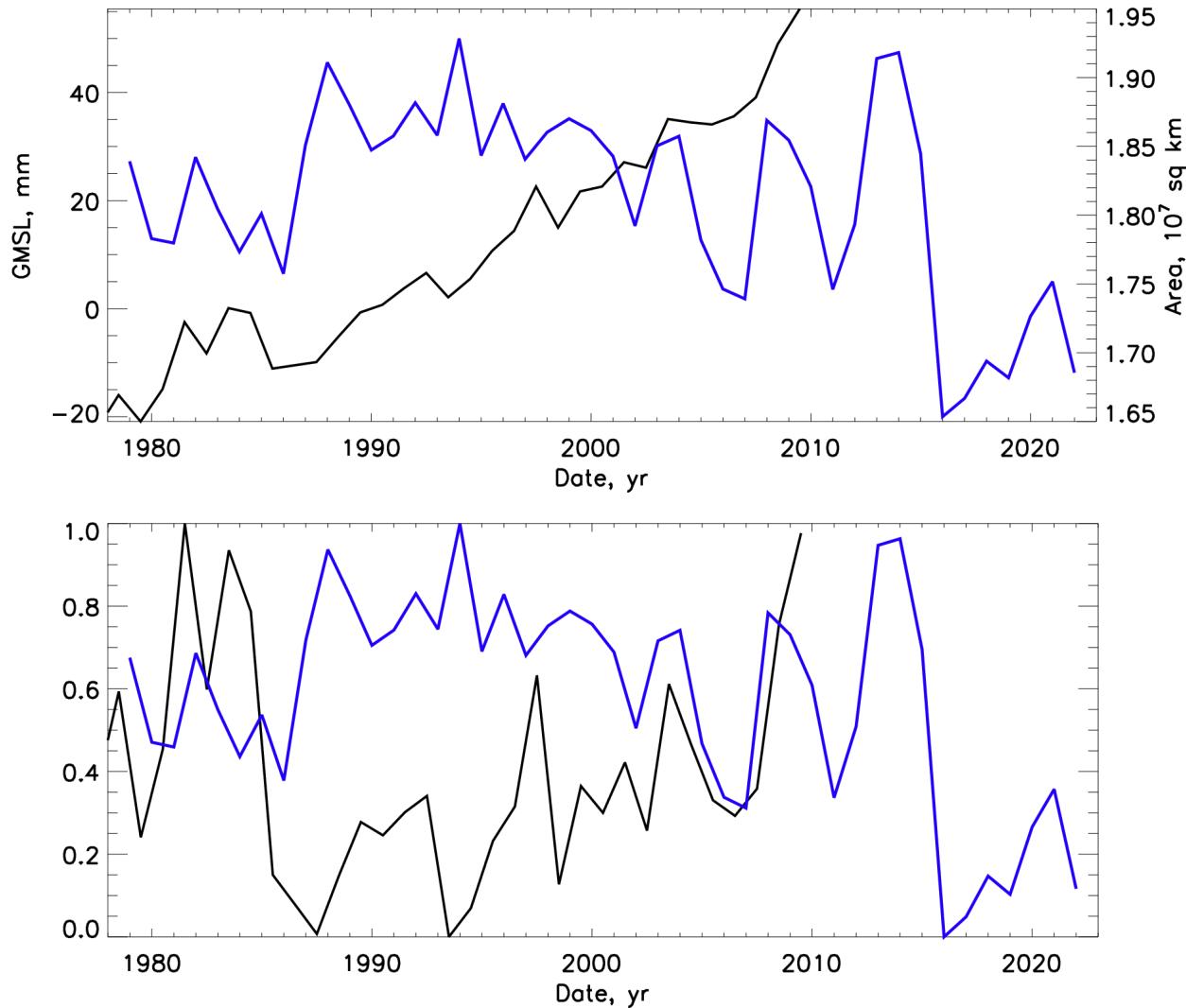
Figure 5:   Top plot: The variations of the sea level of the world ocean (black curve) versus the aggregate ice ares of the Northern and Southern hemispheres (blue curve). Bottom plot - same as above but with the de-trended sea level curve revealing the finest level variations calculated by subtracting from the real sea level curve the averaged sea level variations (see the text for details).
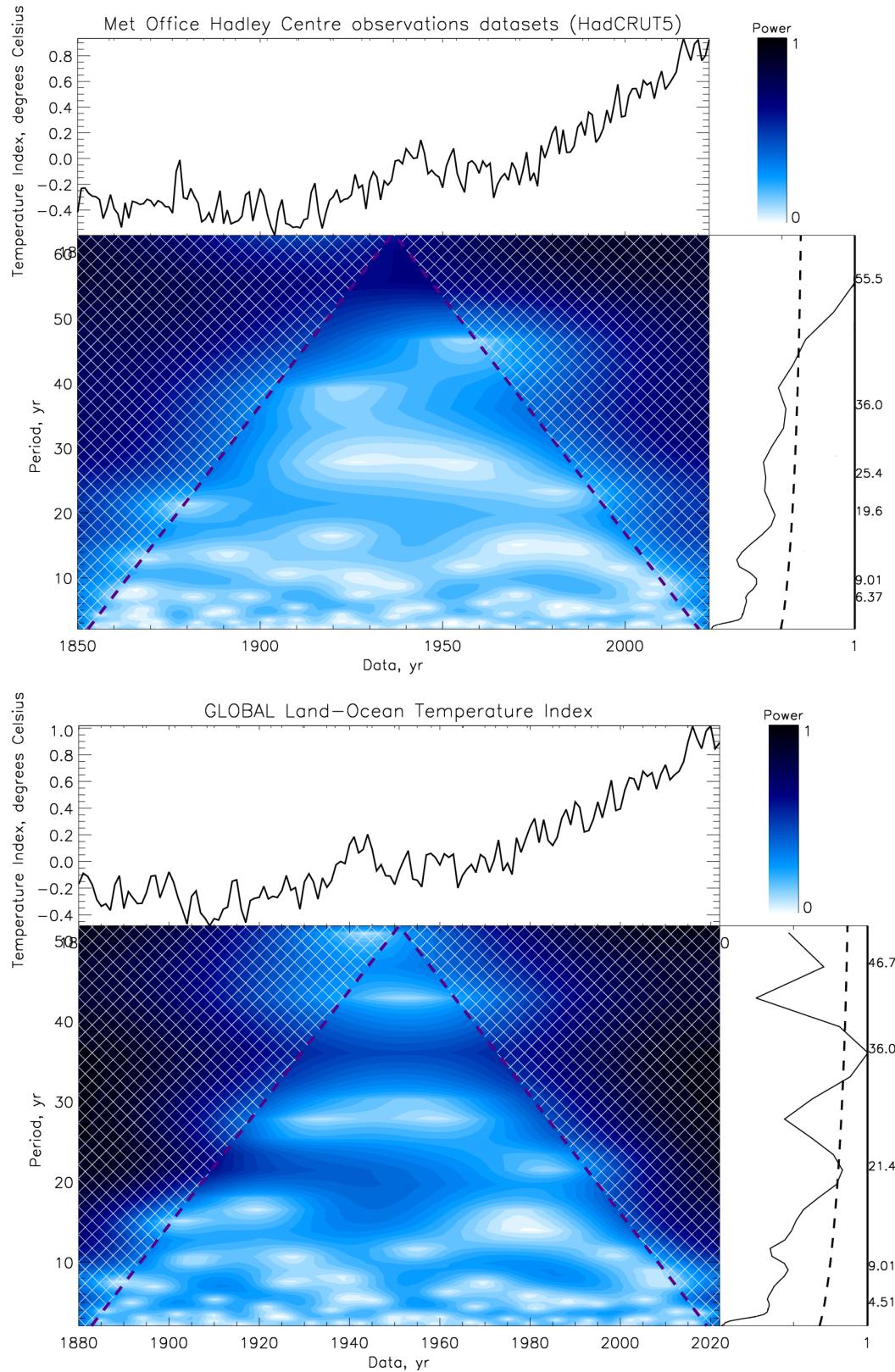
Figure 6: Top plot: The HadCRUTS terrestrial temperature variations (upper line), the wavelet spectrum of the temperature (left bottom plot) with the power marked by the colour bar (the top right plot). The global wavelet spectrum of temperature (black solid line), 95% confidence interval (black dashed line)..
Bottom plot: The GLB terrestrial temperature variations (upper plot), the wavelet spectrum of temperature (bottom plot) with the power marked by colour bar (the top right plot). The global wavelet spectrum of temperature is shown by the black solid line), 95% confidence interval by the black dashed line.
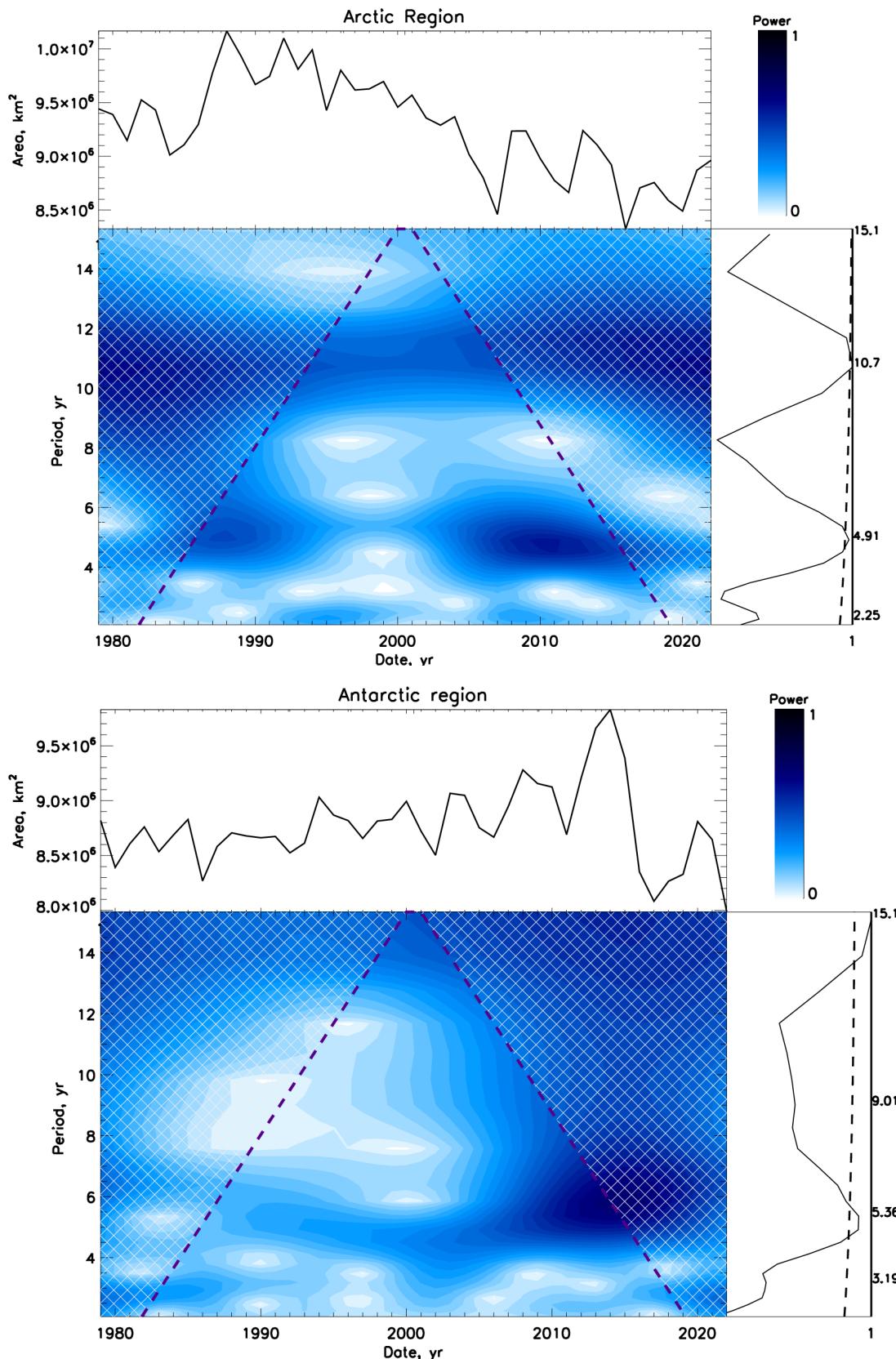
Figure 7: The wavelet spectra of the ice areas in Arctics (top plot) and Antarctica (bottom plot). The global wavelet spectra (black solid line), of ice areas are shown on the right hand side from the wavelet spectra, while the 95% confidence interval is shown by the black dashed line.
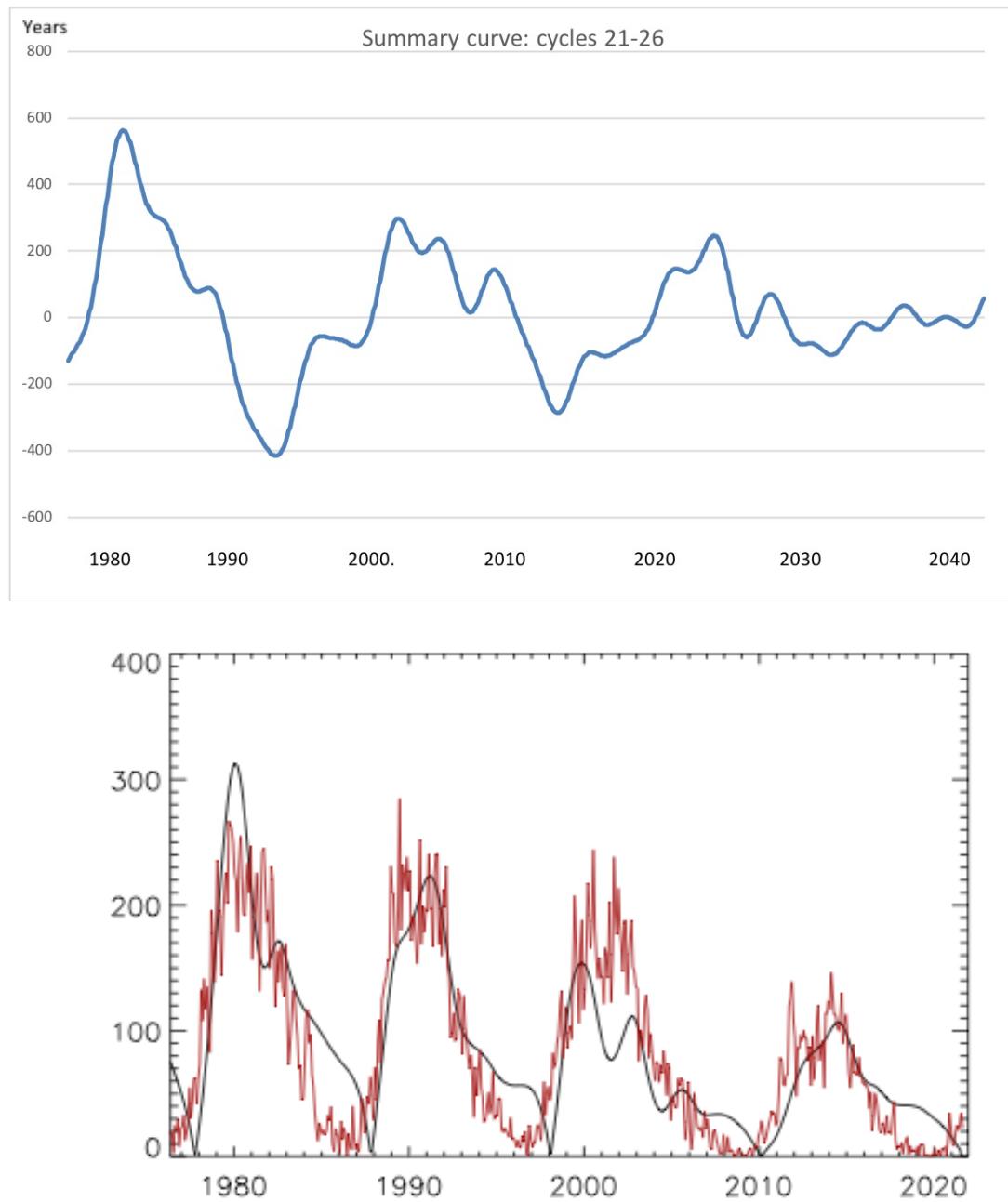
Figure 8: Top plot: The summary curve (in arbitrary units) of two principal components, PCs, for cycles 21-26 derived from the magnetic field data for cycles 21-23 and extrapolated for cycles 24, 25 and 26 (a courtesy of [40]). Bottom plot: Modulus summary curve, in arbitrary units, derived from the summary curve above overplotted on the averaged sunspot numbers in cycles 21-24 used as the current solar activity index (a courtesy of [42]).
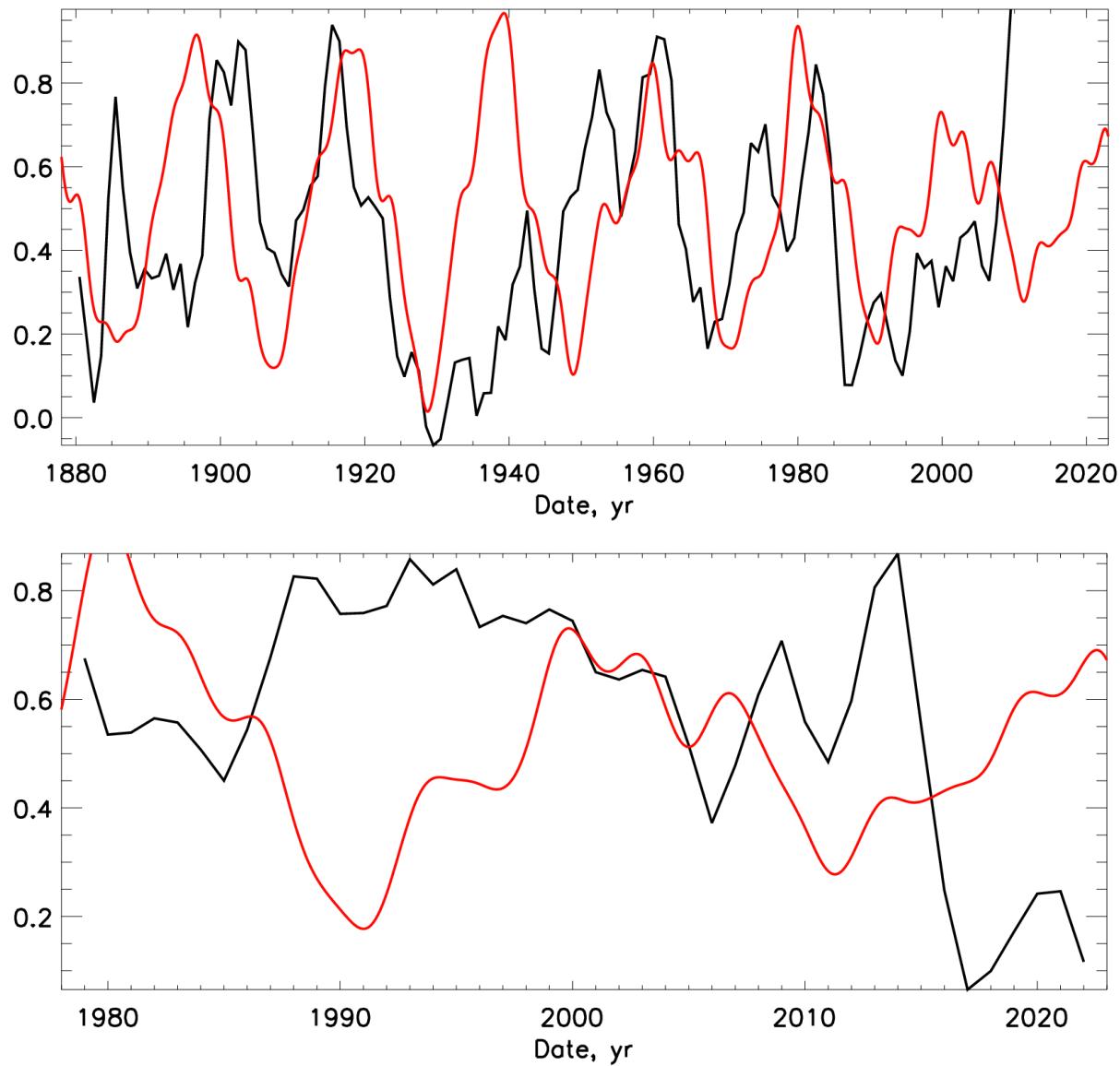
Figure 9: Top plot - The variations of the level of the world ocean level (black line) versus the summary curve of SBMF (red curve) . Bottom plot - The variations of the de-trended total ice areas in both hemispheres (black curve) versus the summary of the SBMF (red curve) (see the text for details).
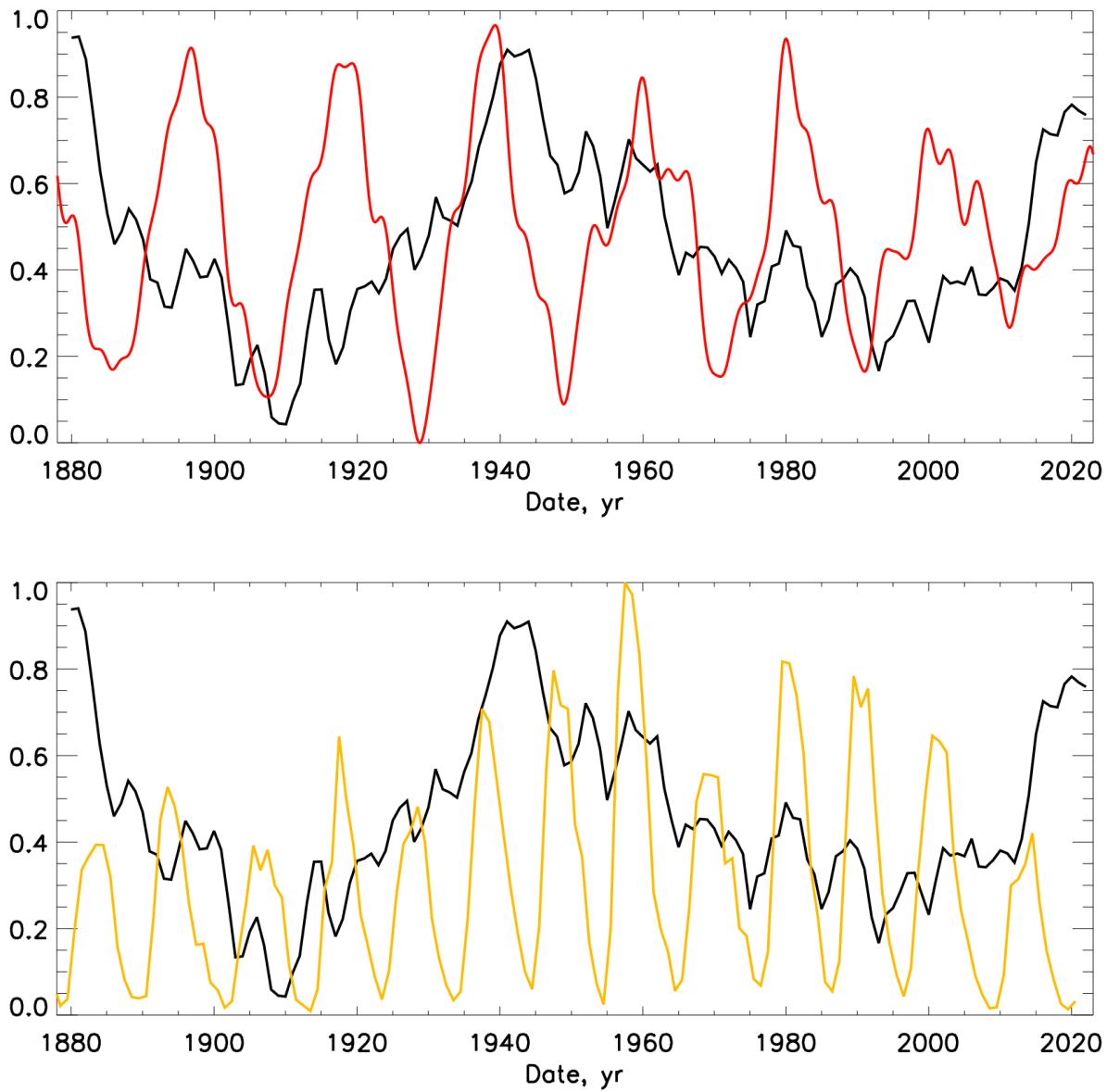
Figure 10: Top plot - The variations of a level of the terrestrial temperature (black curve) versus the summary curve of SBMF (red curve). Bottom plot - The variations of the temperature (black curve) versus versus the averaged sunspot numbers (yellow curve).
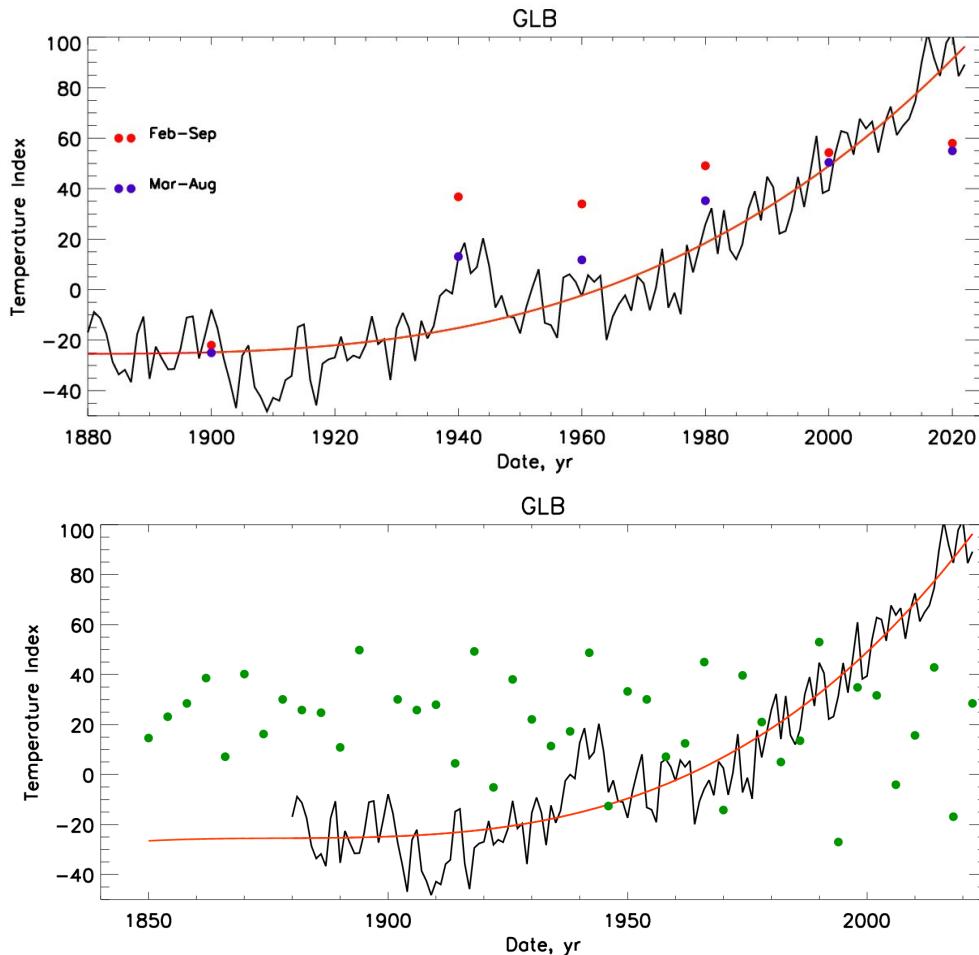
Figure 11: Top plot: The terrestrial temperature variations (black line) and averaged temperature (red line) versus the total solar irradiance (TSI) of the Sun affected by SIM in the spring- summer months as per the legend on the plot. Bottom plot: The temperature plot as above. The dots show the annual total solar irradiance affected by SIM averaged for every 4 years including the leap years. The solar irradiance is calculated by adding the daily irradiance for given spring-summer months in the Northern hemisphere when the Sun is closest to the Earth's orbit [51].